



Test Equipment

Design of a modified three-rail shear test for shear fatigue of composites

I. De Baere*, W. Van Paepelgem, J. Degrieck

*Faculty of Engineering, Department of Mechanical Construction and Production, Ghent University,
Sint-Pietersnieuwstraat 41, B-9000 Gent, Belgium*

Received 5 November 2007; accepted 17 December 2007

Abstract

There are various ways of determining the static in-plane shear properties of a fibre-reinforced composite. One of them is the standard three-rail shear test, as described in “ASTM D 4255/D 4255M The standard test method for in-plane shear properties of polymer matrix composite materials by the rail shear method”. This setup, however, requires drilling holes through the specimen. In this study, a new design based on friction and geometrical gripping, without the need of drilling holes through the composite specimen is presented. Quasi-static tests have been performed to assess the symmetry of the setup and the occurrence of buckling. Then, fatigue tests were done to assess the behaviour of the grips under fatigue loading conditions, yielding excellent results; the specimen fails under shear loading conditions in the loaded area. The material used to validate this setup was a carbon fabric-reinforced polyphenylene sulphide.

During fatigue, this material shows an increase in permanent deformation and a decrease in shear stiffness until a certain point in time, after which a drastic increase in deformation and temperature, higher than the softening temperature of the matrix occurs. Furthermore, the maximum value of the shear stress for fatigue with $R = 0$ has a large influence on the fatigue lifetime.

© 2007 Elsevier Ltd. All rights reserved.

Keywords: Design; Three-rail shear test; Fatigue; Composites

1. Introduction

There are various ways of inducing a state of in-plane shear [1,2] in a composite. Examples are the Iosipescu test [1,3–5], the 10° off-axis test [4–7], the [+45°/−45°]_{ns} tensile test [7–12], the two-rail shear test [13–15], the three-rail shear test [16], torsion of a rod [17] and torsion of thin-walled tubes [18–21]. Of

all of these tests, torsion of a thin-walled tube is practically the only universal method used for determination of both in-plane shear modulus and shear strength [1] and it produces the most desired state of shear stress, free of edge effects [16]. However, this method is rather expensive, since it requires a tension–torsion machine with specialised gripping and it cannot determine the shear characteristics of flat products, fabricated by pressing or contact moulding. Furthermore, such tubes are not easily fabricated. The [+45°/−45°]_{ns} tests do not require any specialised fixtures, and as such are a lot

*Corresponding author. Tel.: +32 9 264 32 55;
fax: +32 9 264 35 87.

E-mail address: Ives.DeBaere@UGent.be (I. De Baere).

less expensive. On the other hand, they are very sensitive to edge effects due to the $[+45^\circ/-45^\circ]$ lay-up [16]. For the 10° off-axis tests, oblique end tabs are required [4–7].

The rail shear test positions itself somewhat in the middle. It does not require a sophisticated apparatus like the torsion setup and it induces a stress state that does not differ a lot from pure shear. Furthermore, it requires flat specimens with limited preparation.

If fatigue loading conditions are required, then the rail shear test is only rarely considered [16]. The favourite test setup remains the torsion of thin-walled tubes, sometimes combined with tension or bending in biaxial fatigue [18–21]. The $[+45^\circ/-45^\circ]_{ns}$ test is also used [9] for fatigue research.

The rail shear test, both two-rail and three-rail, as described in the “ASTM D 4255/D 4255M The standard test method for in-plane shear properties of polymer matrix composite materials by the rail shear method”, has one large disadvantage: it requires drilling holes through the specimen, so that the clamps can be bolted to the specimen. Drilling in composites should be avoided, since it nearly always causes damage to the composite and it may cause stress concentrations around the holes [14]. Furthermore, the preparation of the specimen takes more time. With this in mind, there has already been a proposal of a new design for the two-rail shear test, described by Hussain and Adams [14,15]. This design no longer requires holes in the specimen.

In this manuscript, a modification for the three-rail shear test is proposed, which no longer requires holes through the specimen, as has been proposed

for the two-rail shear test in Refs. [14,15]. Furthermore, this design should allow for fatigue loading conditions, which were not considered by Hussain and Adams [14,15]. The setup used by Lessard et al. [16] for their fatigue research was the standard three-rail setup, which requires the holes. The emphasis of their study was the use of notched specimens, in order to avoid preliminary failure of the specimens.

Finally, the rail shear test is often only considered for unidirectional reinforced or cross-ply composites, whereas for this study, a carbon fabric-reinforced thermoplastic, namely polyphenylene sulphide (PPS) is considered.

In the next section, the principle of a three-rail shear test is briefly summarised. Then, the design of the new clamps is discussed. This is followed by the quasi-static and fatigue experiments done to assess the behaviour of the setup. Finally, some conclusions are drawn.

2. Principle of the three-rail shear test

The principle of the three-rail shear test is illustrated in Fig. 1(a) and (b). The specimen is gripped by three rails and, during the test, the central rail has a relative vertical motion with respect to the two outer rails. This movement can be either up or down. As a result, a state of shear stress is induced in the specimen.

Fig. 1(b) illustrates the (theoretically) induced deformation state. Near the edges and near the clamps, the stress and deformation state will be slightly different because of the edges and corresponding edge effects.

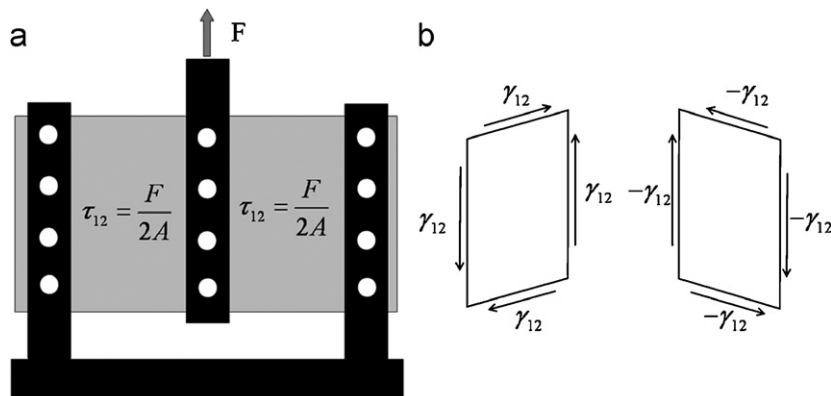


Fig. 1. Principle of the three-rail shear test: (a) the setup and (b) the induced deformation.

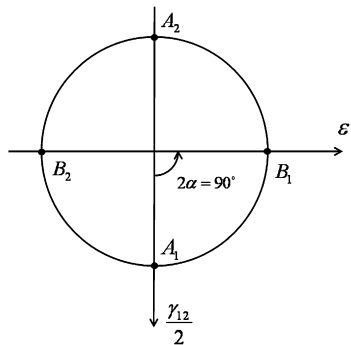


Fig. 2. Representation of the deformation state on Mohr's circle.

The shear stress can be calculated by dividing half of the force (each zone carries half of the total force) by the cross-section:

$$\tau = \frac{F}{2} \times \frac{1}{ht}, \quad (1)$$

where h is the height of the specimen, t is the thickness and F is the imposed force on the central rail.

To measure the shear strain, the ASTM D 4255/D 4255M standard prescribes the use of strain rosettes, but if the loading is symmetrical and no bending of the specimen occurs, even one simple strain gauge will suffice. This can be visualised by presenting the deformation state, given in Fig. 1(b) on Mohr's circle (Fig. 2).

Points A_1 and A_2 correspond with the occurring deformation, a state of pure shear. Rotating over $2\alpha = 90^\circ$ on Mohr's circle to points B_1 and B_2 yields the principal in-plane strains, which can be measured with strain gauges. This corresponds with a rotation of $\alpha = 45^\circ$ on the surface of the specimen for B_1 and of $\alpha = 135^\circ$ for B_2 , meaning that the strain gauges should be mounted under an angle of $+45^\circ$ and -45° with respect to the fibre orientation. The shear strain is then calculated as

$$\gamma = |\varepsilon_{+45} - \varepsilon_{-45}|. \quad (2)$$

If only one strain gauge is mounted, then the shear strain can even be calculated as

$$\gamma = 2|\varepsilon_{+45}|. \quad (3)$$

The latter is also mentioned in Ref. [14], but this assumes symmetry of the loading conditions.

The instrumentation used for this manuscript is discussed in Section 4. Next, the new design is commented on.

3. Design of the setup

Since the setup is designed for fatigue loading conditions, some modifications should be made, so that the setup itself does not fail under fatigue loading. Lessard et al. had also made some modifications to the standard three-rail shear setup [16]. However, for the design presented here, the modifications are far more drastic, since there are no more bolts through the clamp, holding it together. The same principle as in Refs. [13,14] is used, which means that the specimen is gripped by pressing a plate against the specimen. This pressure is applied by bolts which go through only one side of the clamp. However, the force required to press this load transfer plate against the specimen has a similar but opposite reaction force that pushes the two sides of the grip outwards. The latter effect is clarified in Fig. 3, where the different application of the bolts is illustrated.

It is obvious that because of this outward force, the clamps will need to be more massive if they are to withstand the fatigue loading conditions. As a starting point, the grips are designed in one piece, whereas the standard grips are two separate pieces, bolted together. In the grip, a rectangular cavity is milled away for the specimen. Since sharp corners produce unwanted stress concentrations, circular holes are drilled at the ends of this rectangular cavity to soften the stress concentrations. This results in the grip with a cross-section as illustrated in Fig. 4, with some general dimensions added.

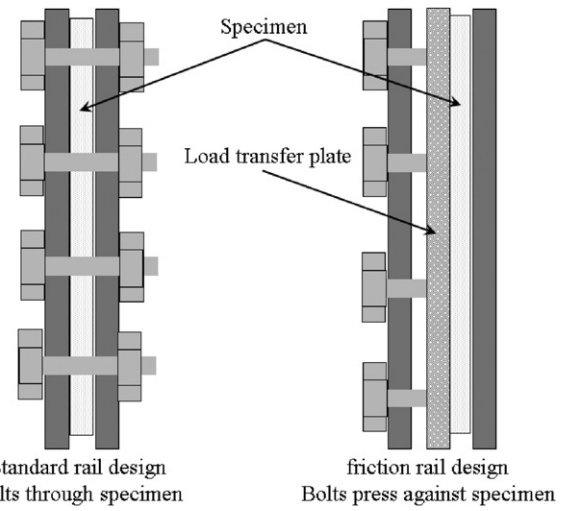


Fig. 3. Difference between the use of bolts in the standard and the new design.

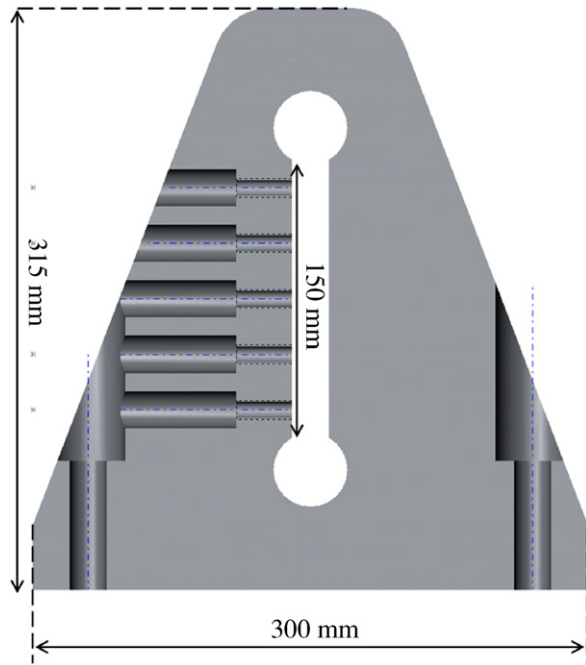


Fig. 4. Vertical cross-section of the grip, indicating some general dimensions.

The design specification stated that the grips should be able to withstand the same dynamic load range as the servo-hydraulic tensile machine it is mounted on. This means that the grips should withstand a longitudinal force of 100 kN. Since the gripping is based on friction, a value of the friction coefficient is estimated. The assumption was made (for design purposes) that a friction coefficient of 0.5 should be feasible, with the use of additional rubber films or layers that increase the friction, should the friction between steel and composite be insufficient.

After a few preliminary tests, it became obvious that for some materials, such as the carbon fabric-reinforced PPS used for this study, a friction coefficient of 0.5 could not be reached, even if extra layers of high friction material were added. In some cases, the rubber film was pushed out of the grips, in other cases, the film failed under the shear loads. This, however, means that the first gripping design, depicted in Fig. 5(a) and based on pure friction, will not suffice. Therefore, geometrical gripping was added, which is illustrated in Fig. 5(b). The load transfer plate is now supported by flattened cylinders, so that the load transfer to the grip is not only achieved by friction but also by these cylinders.

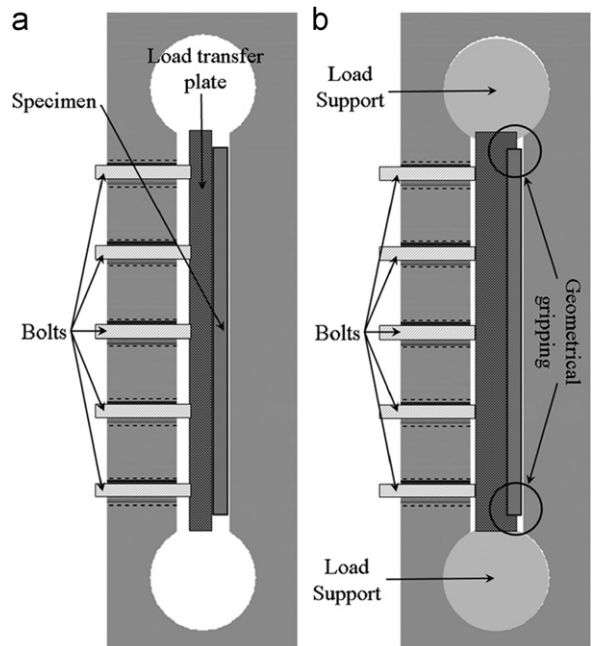


Fig. 5. Illustration of the used gripping principles for the proposed design: (a) only frictional clamping and (b) fraction and geometrical clamping.

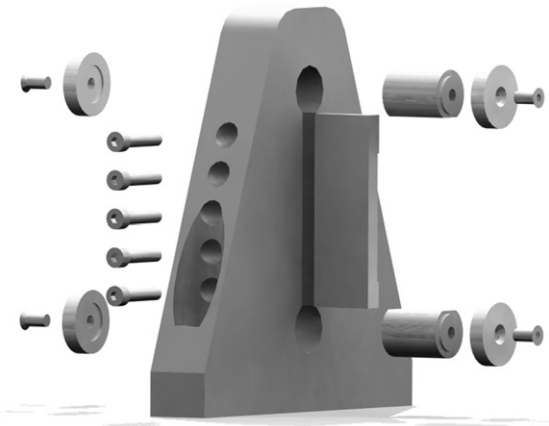


Fig. 6. Exploded view of one clamp for the three-rail shear test.

This final design, implementing both frictional and geometrical clamping, is illustrated in Fig. 6, as an exploded view. This design was used for all experiments conducted in this manuscript.

For the design, the CAD/CAE package “Solidworks 2005” was used. In this package, there is also a finite element module, “COSMOS Express” which was used to determine the stress distribution in the clamp.

In order to ensure an infinite fatigue life under loading of 100 kN, a safety factor of 3 with respect

Table 1
The used material constants in COSMOS Express

| | |
|-----------------------------------|---------|
| Elastic modulus (MPa) | 210,000 |
| Poisson's ratio | 0.28 |
| Yield strength (MPa) | 620 |
| Mass density (kg/m ³) | 7700 |

to the yield stress was taken into account when designing the clamps. Because of the high loads, a high-strength steel was chosen. For the simulation done with the COSMOS Express package, the following material constants for the clamps were used (Table 1).

In this setup, the central clamp carries the highest load; due to symmetry of the three-rail shear setup, each of the outer grips carries half the load of the central one. Therefore, the central grip is considered for the simulations. Furthermore, it is assumed that the vertical force of 100 kN is evenly distributed over the two vertical faces, so that each face carries 50 kN. Using a friction coefficient of 0.5, this results in a necessary horizontal load of 100 kN by the load transfer plate on each face. These loading conditions are the worst case scenario for the grips and assume the use of only frictional gripping (Fig. 5(a)). If geometrical gripping is added (Fig. 5(b)), then the horizontal forces will be less, since part of the vertical force is transported via the cylinders to the grips. As such, the vertical load remains the same, the horizontal force will decrease.

The results of the simulation for the worst case scenario yields the stress distribution depicted in Fig. 7, where the values of the Von Mises criterion are illustrated; the deformation is scaled with a factor of 773.2.

Since the maximum stress level is 154.4 MPa, the minimum factor of safety is 3.86 with respect to the estimated yielding stress of 620 MPa. This should ensure effectively infinite fatigue life.

The clamps were made out of THYROPLAST 2344 EFS steel, which is a quenched and tempered mould steel; the chemical composition is given in Table 2. After quenching, the material has a hardness of 54 HRC and a tensile strength of 1910 MPa. The material has no typical yield behaviour, it is linear until failure. As a result, the safety factor under fatigue loading conditions is a lot higher than 3, ensuring effectively infinite fatigue life. This material was recommended for the highest demands and fitted the request for high strength, high yield stress and high hardness. The latter was

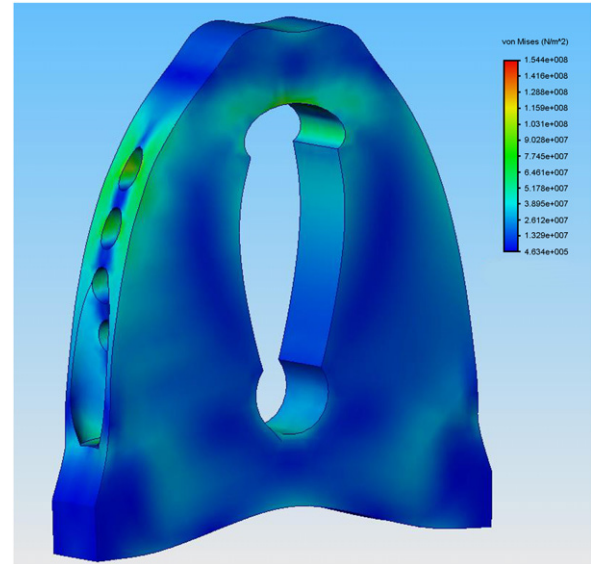


Fig. 7. Von Mises stress distribution in the clamp under the given load conditions. Deformation factor is 773.2 and maximum stress is 154.8 MPa.

Table 2
Chemical composition for the THYROPLAST 2344 EFS, typical analysis in %

| C | Si | Cr | Mo | V |
|------|-----|-----|-----|-----|
| 0.40 | 1.0 | 5.3 | 1.4 | 1.0 |

necessary to avoid damage to the surfaces from glass or carbon fibres.

The DIN material number is 1.2344 and is referred to as X 40 CrMoV 5 1.

After production, the clamps were nitrated for a higher surface hardness, since thermal hardening would result in large, intolerable deformations. The other parts were coated with a (black) nitrate layer with a “niblox” treatment to avoid micro-welding of the surfaces.

Finally, two extra plates were designed in order to be able to mount this setup on a standard servo-hydraulic testing machine. The final setup, mounted on the tensile machine, is shown in Fig. 8.

During fatigue tests, the ram of the tensile machine may start rotating if no precautions are taken. However, this possible rotation of the ram, and therefore the bottom clamp, is inhibited using a special guiding system that is mounted on the ram. Therefore, once alignment of the clamps is



Fig. 8. The final design, mounted on the tensile machine.

achieved, this alignment is guaranteed throughout the fatigue test.

4. Experiments and discussion

4.1. Composite material

The material under study was a carbon fibre-reinforced PPS called CETEX. This material was supplied to us by Ten Cate. The fibre type is the carbon fibre T300J 3K and the weaving pattern is a five-harness satin weave with a mass per surface unit of 286 g/m². The five-harness satin weave is a fabric with high strength in both directions and excellent bending properties.

Table 3

In-plane elastic properties of the individual carbon/PPS lamina (dynamic modulus identification method)

| | |
|----------------|-------|
| E_{11} (GPa) | 56.0 |
| E_{22} (GPa) | 57.0 |
| V_{12} | 0.033 |
| G_{12} (GPa) | 4.175 |

Table 4

Tensile strength properties of the individual carbon/PPS lamina (mechanical testing at TU Delft)

| | |
|---------------------------------|-------|
| X_T (MPa) | 617.0 |
| $\varepsilon_{11}^{\text{ult}}$ | 0.011 |
| Y_T (MPa) | 754.0 |
| $\varepsilon_{22}^{\text{ult}}$ | 0.013 |
| S_T (MPa) | 110.0 |

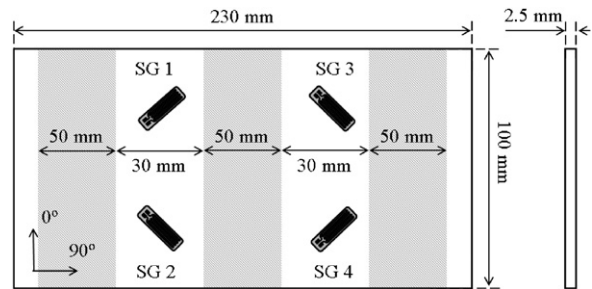


Fig. 9. Dimensions of the used specimen, with a $[(0^\circ, 90^\circ)]_4s$ stacking sequence. The position of the clamps and strain gauges is also illustrated.

The carbon/PPS plates were hot pressed, and only one stacking sequence was used for this study, namely a $[(0^\circ, 90^\circ)]_4s$ where $(0^\circ, 90^\circ)$ represents one layer of fabric.

The in-plane elastic properties of the individual carbon PPS lamina were determined by the dynamic modulus identification method as described in Ref. [22] and are listed in Table 3.

The tensile strength properties were determined at the Technical University of Delft and are listed in Table 4.

The test coupons were sawn with a water-cooled diamond saw. The dimensions of the coupons are shown in Fig. 9.

4.2. Equipment

All tensile tests were performed on a servo-hydraulic INSTRON 1342 tensile testing machine

with a FastTrack 8800 digital controller and a load cell with a dynamic range of ± 100 kN.

For the registration of the test data, a combination of a National Instruments DAQpad 6052E for FireWire, IEEE 1394 and the SCB-68 pin shielded connector were used. The load and displacement, given by the FastTrack controller, as well as the extra signals from the strain gauges, were sampled on the same time basis.

4.3. Quasi-static experiments

The desired stress state for this setup is to have pure and equal shear load for both of the loaded zones. However, due to misalignment of the clamps, the zones on the left and the right of the central clamp may not experience the same load. Furthermore, buckling or bending of the specimen may occur, which means that the front and the back of one loaded zone (left or right) may have a different stress state. Hence, a few quasi-static tests were done to assess the occurrence of buckling and whether the setup induces a symmetrical load. Both types of tests were done in a displacement-controlled manner with a displacement speed of 1 mm/min; the signals were sampled at 20 Hz. Furthermore, quasi-static cyclic loading (hysteresis) was applied, starting with a shear stress of 10 MPa and increasing with 10 MPa each cycle until the

strain gauges saturated or de-bonded. By performing these cyclic loadings, possible problems regarding symmetry or buckling will be more easily detected than in a quasi-static test with monotonic loading until saturation or de-bonding of the gauges, because differences in the strains will probably increase with each successive loading, due to permanent deformation of the specimen.

To verify the symmetry, four strain gauges were placed on the same side of the specimen, but distributed over the two loaded zones, as illustrated in Fig. 9. The time evolution of the different strain gauges for such a test is given in Fig. 10. If the setup is symmetrical, then strain gauges 1 and 3 and strain gauges 2 and 4, respectively, should give the same strain. It can clearly be seen that the signals coincide almost perfectly, meaning symmetry is achieved. The de-bonding or failing of the strain gauges can also be seen: after about 350 s, strain gauge 3 debonded; after 450 s, gauge 1 failed and after 500 s, gauge 2 failed. Gauge 4 failed soon after gauge 2. As a result, the corresponding curves no longer coincide from that point on.

To assess whether buckling occurs, the four strain gauges were placed on the same loaded zone, but on front and rear surfaces. Strain gauges 1 and 2 were placed as depicted in Fig. 9 and strain gauges 3 and 4 were placed in the same position on the opposite side of the specimen in such a way that the strains

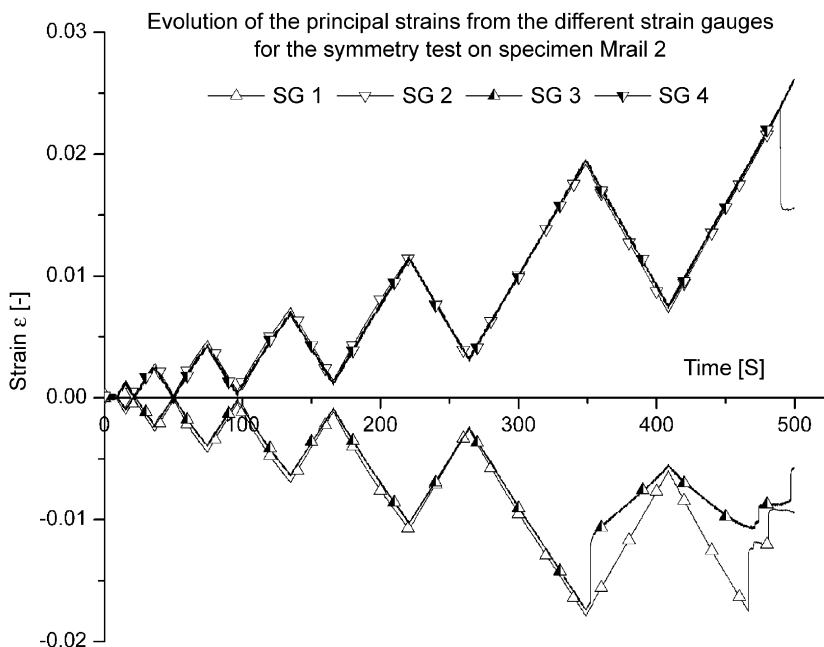


Fig. 10. Evolution of the strain as a function of time for all four strain gauges in the symmetry test.

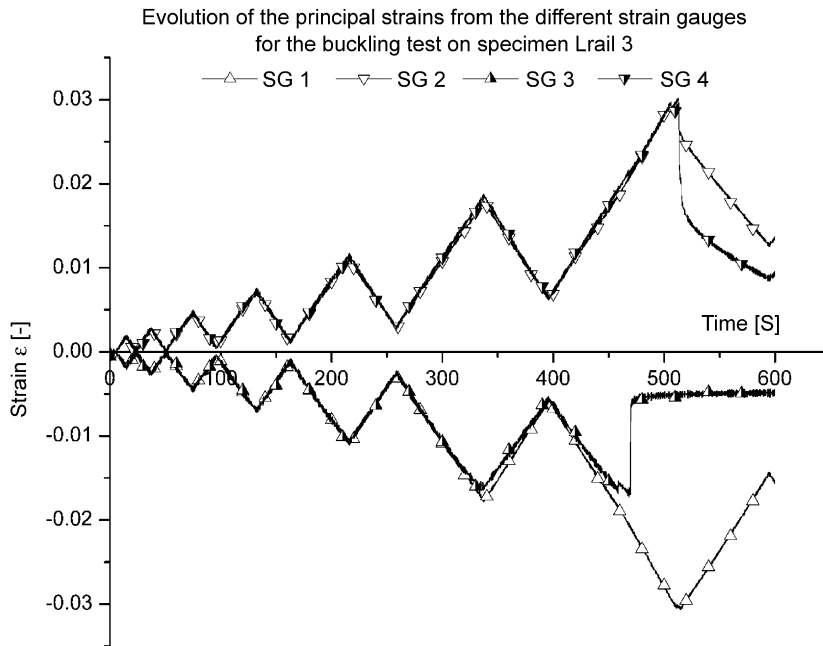


Fig. 11. Evolution of the strains from all four strain gauges as a function of time for the buckling test.

from strain gauges 1 and 2 should correspond with the signals from strain gauges 3 and 4, respectively. The result from such a test is depicted in Fig. 11. Again, the signals coincide almost perfectly. Similar to the previous test, the curves are only shown until the strain gauges de-bonded. This happened at 470 s for gauge 3 and at 510 s for gauge 4. The other gauges failed soon after 600 s.

Similar experiments have been conducted, all with corresponding results. As such, it may be concluded that the stress state induced by the clamps is symmetrical and that no buckling or bending of the specimen occurs. As a result, there is no longer need for four strain gauges, two strain gauges, mounted on the same surface of one loaded zone under $+45^\circ$ and -45° suffice for the measurement.

For both measurements mentioned earlier, the temperature was also monitored, using a thermocouple. Because of the shear loads, a temperature increase is expected. However, no significant increase in temperature was detected.

To verify the evolution of the shear stress as a function of the shear strain, two quasi-static tests, instrumented with strain gauges, were done. For comparison, a quasi-static tensile test, as described by the "ASTM D 3518-76 Standard practice for in-plane shear stress-strain response of unidirectional reinforced plastics" was done on a $[(+45^\circ, -45^\circ)]_{4s}$ specimen. The results are shown in Fig. 12, the

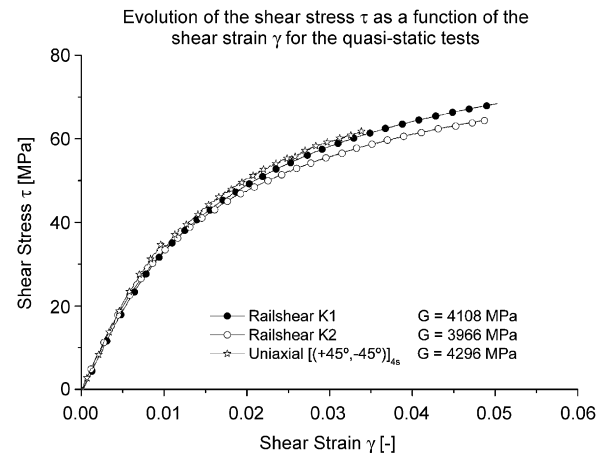


Fig. 12. Shear stress-strain evolution for the quasi-static rail shear tests. A uni-axial test according to the ASTM D 3518-76 is added for comparison.

curves are depicted until the strain gauges either de-bonded or saturated. It must be noted that these curves correspond well, even for the uni-axial test on the $[(+45^\circ, -45^\circ)]_{4s}$ specimen. The shear stiffness is found by taking the tangent modulus in the origin. It must be noted that these values show good correspondence with the value determined by the dynamic modulus identification method (Table 3). Since four strain gauges were mounted on the rail shear specimens, two shear

stress-strain curves could be calculated. However, in Fig. 12, only the curve from the strain gauges that lasted the longest (de-bonding or saturation) is shown. As a result, the maximum shear strain depicted in the graph is not the failure strain. For the rail shear specimens, the tests were stopped after the gauges de-bonded to assess the permanent deformation after unloading and to keep the specimen intact for further non-destructive testing. The $[(+45^\circ, -45^\circ)]_{4s}$ specimen, however, was loaded until failure occurred at 105 MPa, which is in good correspondence with the value from Table 4.

Because of the combined frictional and geometrical clamping of the design, this setup has another interesting advantage. Given the definition of the

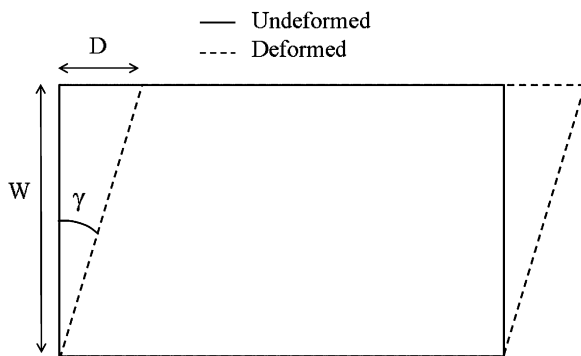


Fig. 13. Definition of the shear strain γ .

shear strain γ (Fig. 13), it can be calculated as

$$\tan \gamma = \frac{D}{W}. \quad (4)$$

If small displacements are assumed, the shear strain will be small and can be calculated as

$$\tan \gamma \approx \gamma \approx \frac{D}{W}. \quad (5)$$

This means that there should be a linear correlation between the shear strain γ and the imposed displacement from the central rail D , given by ($W = 30 \text{ mm}$, see Fig. 9)

$$\gamma = (1/30)*D = 0.033D. \quad (6)$$

During the experiments, it was noted that there is a correlation between the imposed displacement and the resulting shear strain in the specimen, but it is parabolic rather than linear. This is illustrated in Fig. 14; the different experiments are given an offset along the x -axis for a clear image. It can be noted that for both the hysteresis tests, the curves are very reproducible.

The reason for the difference between the experimental and theoretical correlation can be explained as follows. Theoretically, a displacement of 2 mm on the side edge is exactly 2 mm, whereas a displacement of 2 mm of the ram will be less than 2 mm displacement of the side edge of the loaded zone, because of the following reasons: (1) the height of

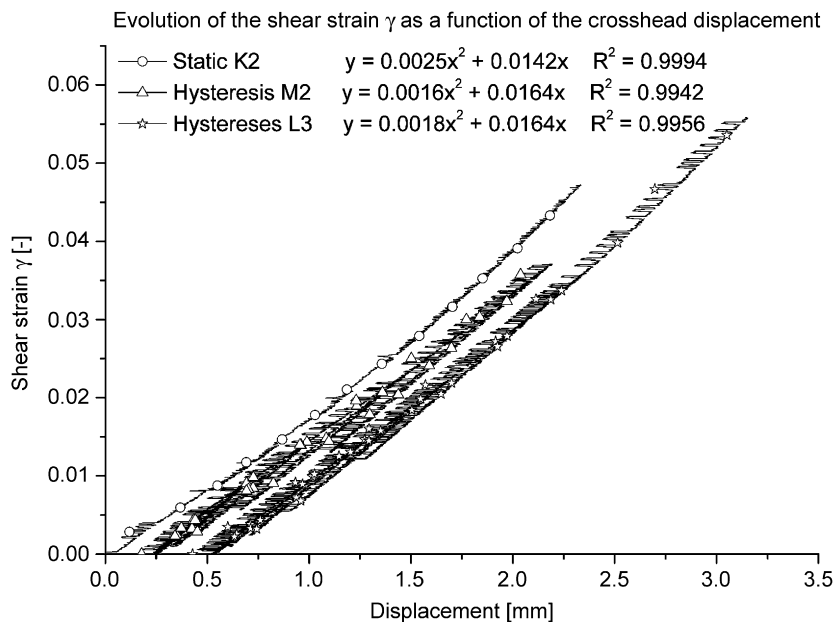


Fig. 14. Illustration of the correlation between shear strain and displacement.

the specimen is not exactly equal to the height of the geometrical gripping, since mounting the specimen would then be practically impossible. As a result, some slippage may occur. (2) The load transfer plates do not fit exactly in the space provided, the height is a little less, since otherwise the plates could not be mounted. Again, some slippage may occur. (3) The mounting mechanism on the tensile machine, as well as the tensile machine itself, deforms under the occurring loads. Hence, the displacement of the side of the specimen will always be a little less than the imposed displacement by the ram. This is the same reason as why the calculated strain from the displacement in a uni-axial tensile test differs from the strain measured with extensometer or strain gauges.

Of course, after some time, enough sliding will have occurred and all free space will be occupied, so for higher displacements, this effect should no longer be present. For instance, if the slope is calculated for specimen L3 for a displacement of 3 mm, this yields

$$\frac{df}{dx} \Big|_{x=3} = 0.0036x + 0.0164 \Big|_{x=3} = 0.0272, \quad (7)$$

which approximates to the expected 0.033. The remaining difference is due to the elastic deformation of the entire setup. This is also the reason why there is a larger difference between the curve for the quasi-static test and the hysteresis tests than between both hysteresis tests. After one loading, there will still be some free space that allows sliding, whereas after a few successive loadings this free space will no longer exist.

It is expected that a similar phenomenon is present when using the standard three-rail shear test setup. However, nothing on this matter is documented by Lessard et al. [16].

Next, finite element simulations have been performed to verify stress distributions and possible stress concentrations. For these simulations, only the loaded part of the specimen was modelled and because of symmetry, only half of the specimen was drawn. Fig. 15 depicts the mesh and boundary conditions used.

The specimen was meshed using a 3D quadratic brick element with reduced integration; the size of the mesh was 3 mm and eight elements through the thickness were used. An extra simulation was performed with a mesh size of 1 mm, but this did not yield different results, it only increased the required calculation time. As such, all simulations

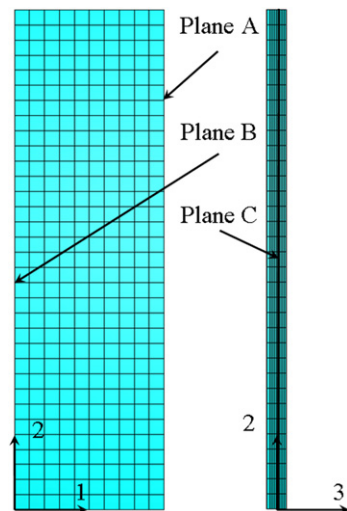


Fig. 15. Used mesh for the finite element simulations.

discussed here use the 3-mm mesh. The width of the modelled specimen was 30 mm and the height 100 mm, as was the case in the experiments. The following boundary conditions were applied:

- Plane A, the right side of the loaded zone, was fixed along the 1- and 2-axis.
- Plane B, the left side of the loaded zone, was fixed along the 1-axis and given a displacement of 3 mm along the 2-axis. This value corresponds with the value at which point the strain gauges in the experiments de-bonded or saturated.
- Plane C, the central plane of the loaded zone, was fixed along the 3-axis.

Since it is a 3D analysis, there are no rotational degrees of freedom. Because of the large deformations, a geometrically non-linear simulation was performed. In Fig. 16, the calculated relation between shear strain and displacement is depicted, as verification for the theoretical deduction above. It can be seen that there is a slight difference, possibly because in the theoretical deduction small displacements were assumed, whereas this simulation has taken geometrical non-linearities into account.

To assess the effect of the boundary condition on this factor, a second simulation was performed, using the same boundary conditions as in Ref. [16], which means that for plane A, only zero displacement along the 2-axis was prescribed (BC2). This, however, does not seem to have any influence on the shear strain–displacement relationship.

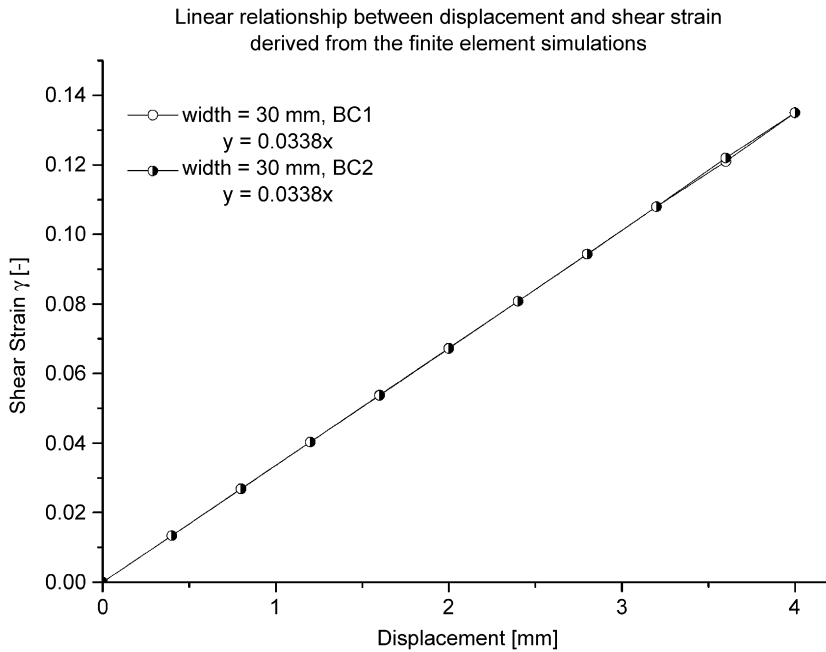


Fig. 16. Numerical evolution of the shear strain as function of the displacement.

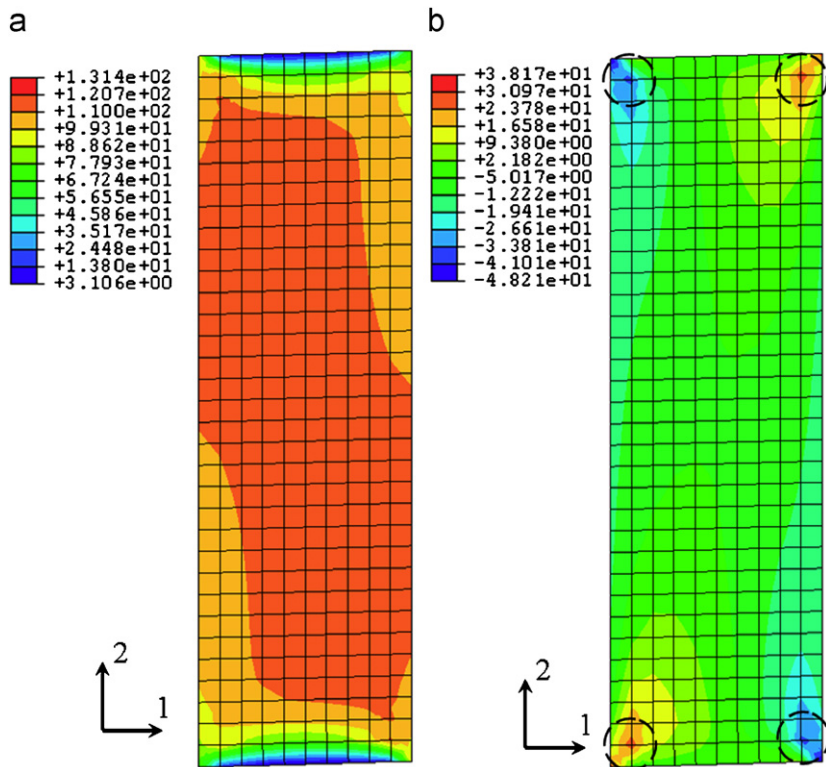


Fig. 17. Distributions of the shear stress and fibre stress in the specimen: (a) shear stress τ_{12} [Mpa] and (b) fibre stress σ_{11} [Mpa].

Finally, the stress distributions from the finite element simulations are shown in Fig. 17 for the original boundary conditions. Apart from the

stresses near the free edges, a very uniform shear stress state is imposed. Stress concentrations for the stresses along the horizontal axis (σ_{11}), however, do

occur. Since no material model is used for these simulations, the shear stresses already reach high values for low displacements. It is expected that if the non-linear material behaviour, as depicted in Fig. 12, is implemented in the simulations, an even more uniform stress state will be achieved.

4.4. Fatigue experiments

Since the design has proven to provide reliable and reproducible results, fatigue experiments are considered. Because of the large displacements, these tests were done without strain gauges, since they would de-bond after a few dozen cycles. However, an estimation of the occurring shear strain levels can still be made, because of reproducible correlation between shear strain and displacement for the hysteresis tests. As result, the evolution of the shear strain will be similar to that of the displacement.

Besides load and displacement, the temperature was also monitored during the experiment. Every 5 min five loading cycles were recorded and, from these signals, the maximum, minimum and average values were calculated.

A first load-controlled fatigue test was done with the shear stress between 0 and 40 MPa ($R = 0$) at a frequency of 2 Hz. The maximum shear stress is about 36% of the shear strength. The results are

given in Fig. 18. It should be noted that there is a gradual increase of both the mean value of the displacement and its amplitude. Given the fact that it was a load-controlled test, this means that permanent deformation and shear stiffness reduction occurs. At a certain point in time, around 1,150,000 cycles, the slope of the displacement curves starts increasing and little later there is a significant rise in temperature. The softening temperature of the polyphenylene matrix is 90 °C, but even before this temperature is reached, very large displacements occur. This can probably be explained by the fact that the temperature is registered at the surface of the specimen and the temperature inside the specimen will be higher, since the surface is cooled by the surrounding airflow. Because of the very large displacements and large increase in temperature, the test was stopped before failure at 1,396,165 cycles.

Again, because of the linearity between shear strain and displacement, the same conclusions as for the displacement could be made for shear strain.

A second load-controlled test was done, but at a slightly higher maximum shear stress. This test was done at 2 Hz and between 0 and 45 MPa ($R = 0$), the latter is about 40% of the shear strength. The corresponding results are shown in Fig. 19. The same remarks concerning the displacement and temperature as for the previous test can be made,

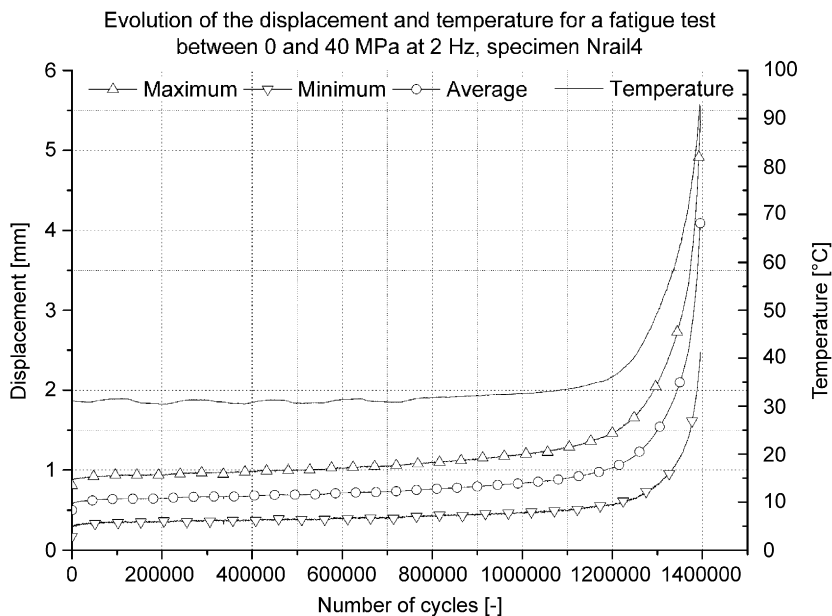


Fig. 18. Maximum, minimum and mean values of the displacement as a function of the number of cycles for a 0–40 MPa fatigue test at 2 Hz.

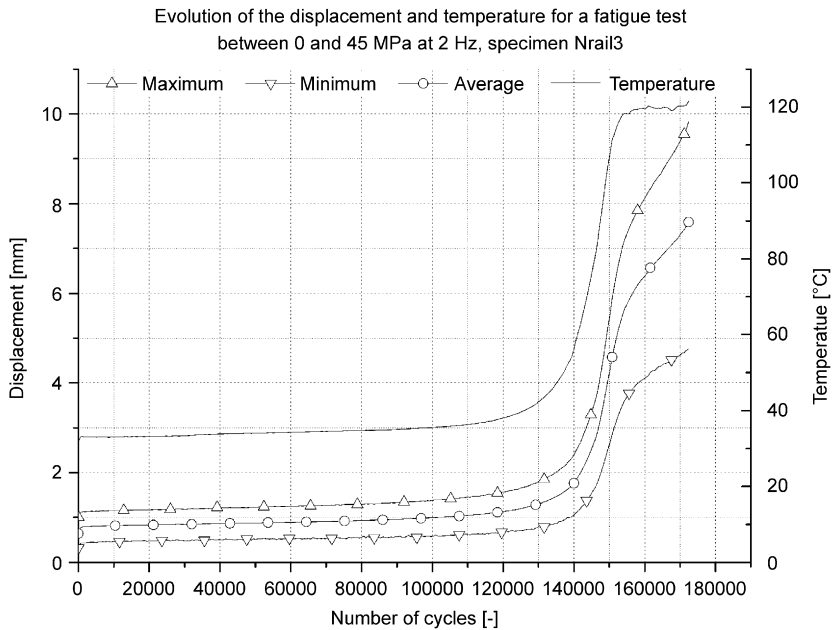


Fig. 19. Maximum, minimum and mean values of the displacement as a function of the number of cycles for a 0–45 MPa fatigue test at 2 Hz.

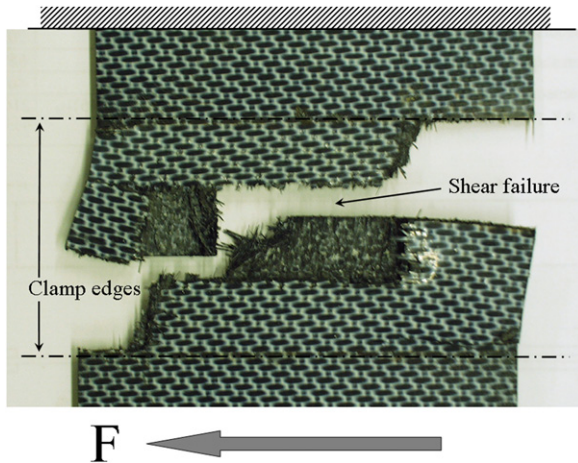


Fig. 20. Illustration of a failed specimen under fatigue loading conditions.

but it should be noted that these effects start a lot earlier. The increase in temperature and displacement occurs after only 130,000 cycles, which is a lot less than the 1,150,000 cycles from the previous test, and this only from an increase in maximum load of 5 MPa. This specimen failed overnight, so it was not stopped before failure, and as a result, a temperature of 120 °C was reached at the surface of the specimen. The resulting softening of the matrix of course causes the large deformations.

Finally, an image of a failed specimen is given in Fig. 20, the position of the clamp edges is also marked. It should be noticed that, although fracture initiated near the clamp ends on the side of the specimen, in the vicinity of the stress concentrations (Fig. 17b), final failure occurred in the shear-loaded zone in the middle of section.

5. Conclusions

A modified design of the standard three-rail shear setup, as described in “ASTM D 4255/D 4255M The standard test method for in-plane shear properties of polymer matrix composite materials by the rail shear method”, has been presented. This new design uses friction and geometrical gripping, without the need of drilling holes through the composite specimen. Quasi-static tests to assess the symmetry of the setup and the occurrence of buckling have been performed with very good results; both sides of the specimen are loaded symmetrically and no buckling occurs. The shear stiffness derived from the static tests is in good correspondence with the stiffness determined by the dynamic modulus identification method and the $[(45^\circ, -45^\circ)]_{4s}$ test. Finally, fatigue tests have been performed to assess the behaviour of the grips under fatigue loading conditions, with excellent results; the specimen fails under shear loading conditions in the loaded area.

The material itself has an increase in permanent deformation and a decrease in shear stiffness until a certain point in time, after which a drastic increase in deformation and temperature occurs. The latter exceeds the softening temperature of the polyphenylene matrix. The maximum value of the shear stress amplitude for fatigue with $R = 0$ has a large influence on the fatigue lifetime.

Future work will concentrate using this new setup for modelling the shear behaviour of the carbon fabric-reinforced polyphenylene sulphide, both under quasi-static and fatigue loading conditions.

Acknowledgements

The authors are highly indebted to the university research fund BOF (Bijzonder Onderzoeksfonds UGent) for sponsoring this research and to Ten Cate Advanced Composites for supplying the material.

References

- [1] Y.M. Tarnopol'skii, A.K. Arnautov, V.L. Kulakov, Methods of determination of shear properties of textile composites, *Compos. Part A—Appl. Sci. Manuf.* 30 (7) (1999) 879–885.
- [2] J.M. Whitney, I.M. Daniel, R.B. Pipes, *Experimental Mechanics of Fiber Reinforced Composite Materials. Composite Characterization (Chapter 4)*, The Society for Experimental Mechanics, Connecticut, 1984, pp. 160–202.
- [3] E.M. Odom, D.M. Blackketter, B.R. Suratno, Experimental and analytical investigation of the modified Wyoming shear-test fixture, *Exp. Mech.* 34 (1) (1994) 10–15.
- [4] G. Odgaard, M. Kumosa, Determination of shear strength of unidirectional composite materials with the Iosipescu and 10° off-axis shear tests, *Compos. Sci. Technol.* 60 (2000) 2917–2943.
- [5] F. Pierron, A. Vautrin, New ideas on the measurement of the in-plane shear strength of unidirectional composites, *J. Compos. Mater.* 31 (9) (1997) 889–895.
- [6] F. Pierron, A. Vautrin, The 10° off-axis tensile test: a critical approach, *Compos. Sci. Technol.* 56 (1996) 483–488.
- [7] W. Van Paepegem, I. De Baere, J. Degrieck, Modelling the nonlinear shear stress-strain response of glass fibre-reinforced composites. Part I: experimental results, *Compos. Sci. Technol.* 66 (10) (2006) 1455–1464.
- [8] A.T. Echtermeyer, Evaluation of the [± 45]s inplane shear test method for composites reinforced by multiaxial fabrics, in: P.J. Hogg, K. Schulte, H. Wittich (Eds.), *ECCM-CTS 2: Composites Testing and Standardisation*, European Conference on Composites Testing and Standardisation, 13–15 September 1994, Woodhead Publishing Limited, Hamburg, Germany, pp. 305–313.
- [9] S. Shalom, H. Harel, G. Marom, Fatigue behaviour of flat filament-wound polyethylene composites, *Compos. Sci. Technol.* 57 (9/10) (1997) 1423–1427.
- [10] J. Payan, C. Hochard, Damage modelling of laminated carbon/epoxy composites under static and fatigue loadings, *Int. J. Fatigue* 24 (2–4) (2002) 299–306.
- [11] U.A. Khashaba, In-plane shear properties of cross-ply composite laminates with different off-axis angles, *Compos. Struct.* 65 (2) (2004) 167–177.
- [12] T. Maeda, V. Baburaj, T. Koga, Evaluation of in-plane shear modulus of composite laminates using holographic interferometry, *Opt. Eng.* 36 (7) (1997) 1942–1946.
- [13] A.K. Hussain, D.F. Adams, The Wyoming-modified two-rail shear test fixture for composite materials, *J. Compos. Technol. Res.* 21 (4) (1999) 215–223.
- [14] A.K. Hussain, D.F. Adams, Experimental evaluation of the Wyoming-modified two-rail shear test method for composite materials, *Exp. Mech.* 44 (4) (2004) 354–364.
- [15] A.K. Hussain, D.F. Adams, Analytical evaluation of the two-rail shear test method for composite materials, *Compos. Sci. Technol.* 64 (2) (2004) 221–238.
- [16] L.B. Lessard, O.P. Eilers, M.M. Shokrieh, Testing of in plane shear properties under fatigue loading, *J. Reinf. Plast. Compos.* 14 (9) (1995) 965–987.
- [17] L. Ferry, D. Perreux, D. Varchon, N. Sicot, Fatigue behaviour of composite bars subjected to bending and torsion, *Compos. Sci. Technol.* 59 (4) (1999) 575–582.
- [18] A.M. El-Assal, U.A. Khashaba, Fatigue analysis of unidirectional GFRP composites under combined bending and torsional loads, *Compos. Struct.* 79 (4) (2007) 599–605.
- [19] D. Qi, G. Cheng, Fatigue behavior of filament-wound glass fiber reinforced epoxy composite tension/torsion biaxial tubes under loading, *Polym. Compos.* 28 (1) (2007) 116–123.
- [20] H. Kawakami, T.J. Fujii, Y. Morita, Fatigue degradation and life prediction of glass fabric polymer composite under tension torsion biaxial loadings, *J. Reinf. Plast. Compos.* 15 (2) (1996) 183–195.
- [21] T. Fujii, F. Lin, Fatigue behaviour of a plain-woven glass fabric laminate under tension-torsion biaxial loading, *J. Compos. Mater.* 29 (5) (1995) 573–590.
- [22] I. De Baere, W. Van Paepegem, J. Degrieck, H. Sol, D. Van Hemelrijck, A. Petreli, Comparison of different identification techniques for measurement of quasi-zero Poisson's ratio of fabric reinforced laminates, *Compos. Part A—Appl. Sci. Manuf.* 38 (9) 2047–2054.